ELSEVIER

Thin Solid Films 297 (1997) 192–201

thin solid films

Porous anodic alumina: fabrication, characterization and applications

G.E. Thompson

Corrosion and Protection Centre, UMIST, Manchester M60 1QD, UK

Abstract

A review is given of anodic alumina film formation on aluminium, with barrier and porous films developed by anodic polarization in an appropriate electrolyte. Initial consideration of barrier-type films, using marker and tracers, allows definition of the locations of film growth and consideration of the transport processes under the high electric field. From this base, the effects of altering film growth conditions, generally using acid electrolytes, to generate porous anodic films are considered, with be resultant films of defined morphology thickening as a result of the dynamic equilibrium between film growth at the metal–film interface and field assisted dissolution at the pore base–electrolyte interface. Means for characterising the developed films are presented as well as applications of the porous, amorphous film material. © 1997 Elsevier Science S.A.

Keywords: Anodic alumina; Fabrication; Characterization; Electrochemistry

1. Introduction

Anodic films, generally on aluminium, have received significant attention due to their diverse applications which, for example, include dielectrics in aluminium capacitors, keying layers for retention of organic coatings and protection of aluminium substrates from their service environments [1]. Their widespread use has enabled significant focus on fundamental aspects of film growth [2,3], including ionic transport in the largely amorphous anodic oxides under intense electric fields, developed by anodic polarization in suitable electrolytes.

Uniquely, for aluminium, films of controlled morphology may be developed by appropriate selection of electrolyte and film-forming conditions (Fig. 1). Thus, films grown at high current efficiency in largely near-neutral electrolytes at ambient temperatures are highly uniform in thickness and relatively compact; such films are termed barrier films (Fig. 1(a)). In recent years it has been shown that barrier films may develop at current efficiencies of film formation above approximately 60% [4,5]. However, irrespective of the current density, the relatively high field developed across the alumina gives rise to Al^{3+} egress and O^{2-} or OH^{-} ingress through the anodic film.

In acid electrolytes, or selected alkaline electrolytes, the relatively compact barrier-type anodic films on aluminium no longer develop as a result of anodic polarization. Examination of the resultant film at appropriate magnification and resolution reveals a relatively regular porous anodic film

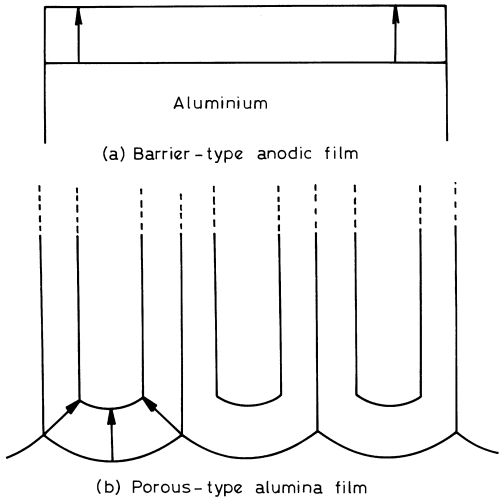

Fig. 1. Schematic diagram showing the section of (a) barrier-type film and (b) porous-type film on aluminium.

(Fig. 1(b)) [6]. The pores, of cylindrical section, pass normally to the macroscopic aluminium surface but are separated from it by a relatively compact barrier layer of scalloped appearance.

For the morphologically-defined barrier and porous-type anodic films, anodizing under specific conditions in various electrolytes allows incorporation of species from the electrolyte, giving compositionally-defined films [7]. Such an ability to control morphology, particularly for porous anodic films, as well as up-take of electrolyte species, enables tailor-making of anodic films for particular applications. For exam-

PII S0040-6090(96)09440

ple, relatively large diameter pores are generated by anodizing at high voltages in phosphoric acid compared with the fine pores in the anodic films which are developed rapidly by anodizing in sulphuric acid.

In this paper, the main theme is porous anodic films on aluminium which includes mechanisms of film growth, pore development and propagation; procedures for determining as precisely as possible the resultant film morphology, composition and structure are also introduced. Finally, applications of porous anodic films are given, including membranes and, keying layers; decorative, wear-resistant and protection treatments for aluminium are also considered.

As indicated previously, the main focus is porous anodic films on aluminium; however, in order to provide the basis for consideration of ionic transport phenomena in amorphous alumina and interfacial processes, initial consideration is given to barrier-type films on aluminium, formed generally, but not exclusively, in near-neutral aqueous electrolytes. The interfacial processes of importance in the formation of a particular film-type proceed at the film–electrolyte or pore base–electrolyte interface, with the ionic migration mechanism within the alumina film awaiting clarification. Relatively recent studies have shown that very significant enrichments of alloying elements may develop over nanoscale dimensions immediately beneath the anodic film [8]. An overview of this behaviour is also presented, since it has broad implications on the surface treatment of aluminium alloys as well as possible relevance to anodic oxidation of electronic materials more generally, i.e. compounds.

In order to provide full coverage of the subject, including experimental details, interpretation and discussion, a series of publications is necessary, involving electrochemical, electron-optical and surface analytical procedures. Consequently, here an overview is given, assisted by use of appropriate schematic diagrams. The information provided has been generated largely in the Corrosion and Protection Centre at UMIST, and due acknowledgement is given to the contributions of colleagues, research assistants and research students; further, the significant contributions of the many workers in this field over considerable periods of time are also acknowledged here.

2. Experimental

For marker and tracer studies during anodizing to produce barrier films and in the growth of porous anodic films generally, spade electrodes of superpure aluminium (impurities: Cu, 0.003 wt.%; Si, 0.002 wt.%; Fe, 0.004 wt.%) are normally employed. Prior to anodizing, various surface pretreatments are used but, in many cases, electropolishing in a perchloric acid–ethanol mixture at 20 V for 5 min at temperatures less than 298 K is employed to develop a reproducible surface finish. Anodizing is then performed at constant current density or constant voltage in various electrolytes of different pH values; the resultant voltage–time or current density–time behaviour, depending on the mode of anodizing, enables the progress of anodic film formation to be followed [9].

Inert xenon marker layers are employed, following the initially successful procedure developed for their direct observation [10], with implantation carried out at an energy of 5 keV and dose of 1×10^{18} ions mm^{-2}. Pre-formed anodic films, of thickness about 12 nm, are developed initially on the electropolished aluminium substrate, allowing the implant to be incorporated almost entirely within the anodic alumina film. Reanodizing, after implantation, revealed the expected voltage–time or current density–time behaviour, indicating little, if any, influence of the implant on the ionic transport processes during reanodizing. The procedure indicated eliminated the anomalous film growth evident for anodizing implanted aluminium and the spreading of the implant region as a result of film growth.

After film growth, various analytical procedures may be employed to characterize film morphology, composition and structure. In the first case, morphological features are observed directly using transmission electron microscopy; thus plan views of the anodic films are made by stripping the film from the scored substrate by amalgamation in mercuric chloride solution. Cross-sections of the anodic film, attached to the aluminium substrate, are generated by ultramicrotomy using LKB, Dupont, RMC or Reichert ultramicrotomes in the usual manner [11]. Briefly, the encapsulated specimens are trimmed initially with a glass knife and final sections, of thicknesses as low as 7 nm, are generated with a diamond knife; the resultant sections are collected from the water bath at the rear of the diamond knife and examined in Philips and Jeol electron microscopes at acceleration voltages between 100 and 200 kV.

Film compositions are determined frequently by Rutherford backscattering spectroscopy of α-particles (and related nuclear methods) using a 7.0 MeV Van de Graaff generator; when necessary and to avoid overlapping yields from the underlying aluminium, window techniques are utilized [12]. Additionally, Auger electron spectroscopy with ion etching and X-ray photoelectron spectroscopy with chemical sectioning are used for in-depth elemental profiles and appropriate valency discrimination respectively [13]; such information is also supported by analytical transmission electron microscopy, with suitable electron probes allowing appropriate resolution and count rate.

Structural probing of the generally amorphous alumina films is undertaken by X-ray absorption studies (XAS) [14] and with magic angle spinning nuclear magnetic resonance (MAS-NMR) [15]. Generally X-ray absorption spectra of films are recorded on various beamlines at the SRS at Daresbury. For example, spectra for Mo, W and Cr edges are recorded in the fluorescence mode, with specimens mounted at an angle of 45° to the incident beam. Acquisition of Al, S and P K-edge data requires the samples to be mounted in ultra high vacuum. The X-ray absorption is measured by recording the total electrons yield as the drain current from

the sample, whilst the incident flux is measured as the drain current from a beryllium foil intersecting the X-ray beam. Model compound data are also generated in the total electron yield mode, with the samples being prepared by grinding and then dispersion on a copper substrate. High resolution ^{27}Al MAS-NMR are obtained at 93.8 M Hz on a Brucker MSL 360 (8 4ST) spectrometer. For NMR analysis, the oxide sample is removed from the aluminium substrate by the amalgamation procedure indicated previously. About 100 mg of film material is necessary for analysis, requiring anodizing of sufficient specimens of appropriate exposed surface area.

In appropriate situations, the aluminium ion concentration in the electrolyte after anodizing, or through film dissolution in the absence of the field, i.e. chemical dissolution, is determined by atomic emission spectroscopy. Aluminium detection limits are of the order of 50–100 ppb using the allied inductively coupled argon plasma facility.

3. Results and interpretation

3.1. Barrier-type anodic alumina films

As indicated previously, the barrier films of Fig. 1(a) are considered initially, to provide the base for understanding the development of the porous anodic alumina film. For galvanostatic anodizing, the resultant voltage–time behaviour (Fig. 2) reveals an initial voltage surge of about 2.0 V, indicative of the prior presence of an air-formed film of thickness 2.5 nm on the electropolished aluminium surface. Thereafter, the voltage rises linearly with time as the relatively compact film thickens uniformly with time. The driving force for film growth is high field ionic conduction [16], which may be expressed simply as $i = A\exp(BE)$, where i is the anodic current density (typically in the mA range), A and B are temperature dependent constants, and E is the field strength (the ratio of the potential drop across the alumina film to the film thickness). Clearly, films grown at constant current density develop at a constant field strength, of the order of 10^6–10^7 V cm^{-1}; further, the reciprocal of the field strength for anodizing of aluminium reveals that the film thickens at about 1.2 nm V^{-1}. In order to maintain the constant field strength, the voltage must increase as the film thickens. The field also serves to provide highly uniform film growth, with the developing film smoothing the roughness of the initial aluminium surface. Uniform film thickening is terminated eventually by dielectric breakdown, with visible sparking observed frequently over the anodic film surface.

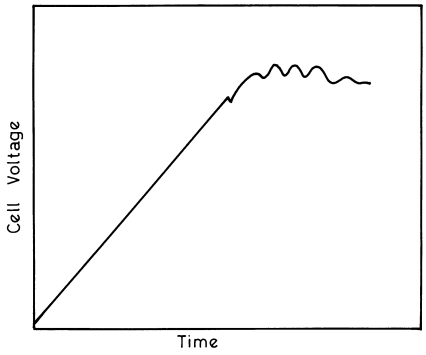

Fig. 2. Schematic diagram of the voltage–time behaviour during anodizing of aluminium at constant current density in neutral solution. The rate of voltage rise at 5 mA cm^{-2} is 2.3 V s^{-1} for anodizing at 100% current efficiency.

3.1.1. Marker and tracer studies

As an initial step in understanding the complex ionic transport processes in amorphous solids, inert marker experiments assist in defining the locations of film growth. Fig. 3 indicates marker locations for transport solely by cation egress (Fig. 3(a)), anion ingress (Fig. 3(b)) and combined cation egress and anion ingress (Fig. 3(c)). For aluminium, anodized under high current efficiency conditions, the last is revealed by transmission electron microscopy of ultramicrotomed sections of anodic films incorporating an immobile and inert xenon marker. The xenon is revealed directly as gas bubbles within the film section; the distribution and uniformity of the xenon has changed little from its presence in the initial pre-formed film. Further, the presence of xenon as discrete bubbles, i.e. not an integral part of the film 'structure', also provides further justification for its immobility. Additional experiments using γ/γ' nuclei as markers confirm the immobility of the xenon marker and the aluminium cation transport number of about 0.4 for film growth at high current efficiency [17]. The cation transport number is determined from the ratio of the film thickness developed above the marker to the total film thickness.

The uniformity of the marker within the film section and its limited spreading across the film thickness also suggest strongly that the alumina film develops simultaneously and only at the film–electrolyte and metal–film interfaces by Al^{3+} egress and O^{2-}/OH^- ingress under the high field, i.e. no growth of film occurs within the film section, which would reveal a non-uniform marker layer distribution.

Tracer studies [18] utilize a mobile species, with its location or distribution within the film determined as a result of an incremental increase in film thickness. A classic example is the determination of ^{16}O and ^{18}O profiles as a result of anodizing initially in a normal aqueous electrolyte, followed

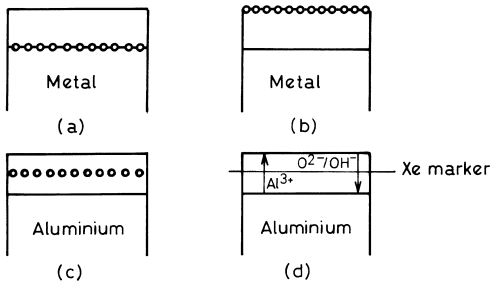

Fig. 3. Schematic diagram of sections of films, revealing location of marker for film growth by: (a) cation transport; (b) anion transport; (c) cation and anion transport; (d) mobile ions for aluminium anodic oxidation.

by reanodizing in a similar, but ^{18}O enriched electrolyte, or vice versa [19]. Broadly, such studies reveal the conservation of the order of oxygen ions, i.e. for anodizing initially in the enriched solution, ^{18}O is present in the inner film regions and extends to the metal–film interface; a separate, distinct O^{16} distribution is evident in the outer film region. On the basis of a similar conservation of the outwardly mobile cations (not yet determined experimentally for aluminium cations), a co-operative transport mechanism of Al^{3+} and O^{2-}/OH^{-} ions has been suggested [3,20]. Progressing further, in order to possibly explain such a mechanism, together with approximately equivalent cation and anion transport numbers, Mott [21] has likened the transport event to a liquid droplet, which involves collective excitation of a small number of ions, possibly 20, such that their vibrations are sufficient for them to act as a liquid. After a time of the order of 10^{-12} s in which they are in this condition, metal and oxygen ions move in opposite directions under the influence of the field. The movement of the these different ions creates a ''frozen-in'' depole, which increases the field acting on neighbouring activated regions.

Given information of the previous kind, detailed consideration of film compositions, has allowed incorporated electrolyte species to be used as markers or tracers, depending upon the nature of the specific contaminant and the influence of the electric field. Concerning film contamination by electrolyte species, e.g. B, W or P species from borate, tungstate or phosphate electrolytes respectively, Auger electron spectroscopy (AES) and secondary ion mass spectrometry (SIMS) enable elemental depth profiling, with chemical sectioning and X-ray photoelectron spectroscopy (XPS) analysis allowing the valence state of the incorporated species to be probed. In addition, XAS, with its sensitive detection limits, valency discrimination and co-ordination determination (along MAS-NMR) from the resultant absorption edge and the near-edge (XANES) and EXAFS spectra, is a powerful probe for incorporation of electrolyte species.

For the anodizing electrolytes indicated, the distributions of electrolyte species are indicated in the schematic diagram of Fig. 4, with B species present over about 0.4 of the film thickness, measured from the film–electrolyte interface (Fig. 4(a)), P species present over two-thirds of the film thickness (Fig. 4(b)), and W species present in the very outer film regions (Fig. 4(c)). For highly efficient film growth and with reference to an inert marker, B species are present in the outer film region developed by Al^{3+} egress (Fig. 4(d)); P species are present in the outer film region and have passed below the marker into the film region developed by O^{2-}/OH^{-} ingress (Fig. 4(e)); W species, like boron species, are present in the film material developed by Al^{3+} egress but, unlike B species, are located only in the outermost film regions (Fig. 4(f)). Confirmation of the previous findings also arises from electron beam induced crystallization of the amorphous alumina film sections in the transmission electron microscope. As a result of electron irradiation, the film regions in which electrolyte species are

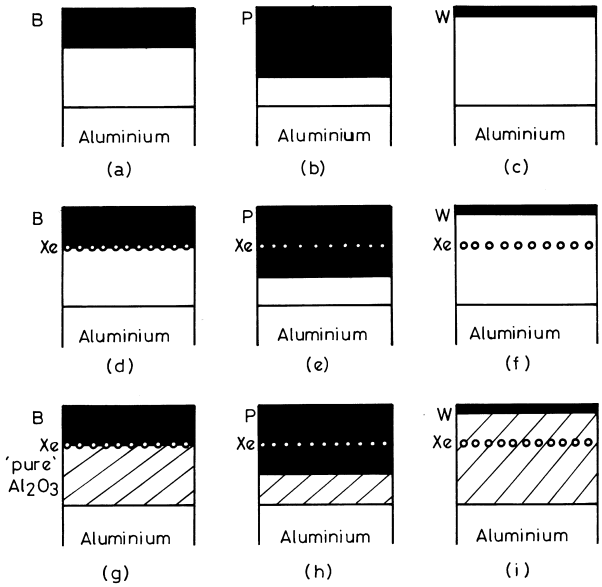

Fig. 4. Schematic diagrams of sections of barrier films formed on aluminium in: (a) borate; (b) phosphate; and (c) tungstate electrolytes. The location of xenon markers are revealed in (d)–(e), and the consequences of differential electron beam induced crystallation (hatched region) in (g)–(i).

absent crystallize more rapidly than the regions doped with electrolyte species. Such differential crystallization of amorphous alumina to γ/γ' alumina thus highlights the inner relatively pure alumina regions, confirming the elemental depth profiles generated by other means (Fig. 4(g) and 4(h)).

In explaining the previous behaviour, direct interpretation suggests immediately that B species are immobile in anodic alumina, P species are mobile inwards and W species are outwardly mobile under the electric field. Progressing further, RBS and related nuclear methods allow precise simulation of film compositions based on the presence of B_2O_3, PO_4^{3-} and W^{6+} species respectively or, in other words, B is present as a neutral species whereas P is present in an inwardly mobile anion form and W is present as an outwardly mobile cation [22].

In order to understand fully the behaviour, detailed consideration of the film–electrolyte interfacial processes is necessary [7,23]. Thus, during film growth, the following reactions are suggested to occur between Al^{3+} ions and adsorbed electrolyte anions at the film–electrolyte interface:

Phosphate solution: $Al^{3+} + PO_4^{3-} \rightarrow AlPO_4$

Borate solution: $2Al^{3+} + H_4B_4O_7^{-} + 2H_2O \rightarrow Al_2O_3 + 2B_2O_3 + 5H^{+}$

Tungstate solution: $2Al^{3+} + WO_4^{2-} + 2H_2O \rightarrow Al_2O_3 + WO_3 + 4H^{+}$

Owing to the relatively low coverage of the film surface by adsorbed anions compared with coverage by water molecules, the main film forming anodic reaction is given below:

$$2Al + 3H_2O \rightarrow Al_2O_3 + 6H^- + 6e$$

The adsorbed anions or resultant electrolyte species are then incorporated uniformly and at relatively low levels into the alumina film material developed by Al^{3+} egress. The fate of the adsorbed/incorporated species within the alumina film material then depends on the consequences of the action of the electric field on the incorporated species. Thus, it is suggested that B_2O_3 units are incorporated, with the electric field strength being insufficient to break B–O bonds, unlike Al–O bonds; hence an immobile species results. Conversely, the field strips oxygen atoms from WO_3, resulting in the generation of W^{6+} cations, which move outwards at a slower rate than that of Al^{3+} ions under the field. For PO_4^{3-} anions, these remain unaffected by the high field and migrate inwards, at a rate less than that of O^{2-}/OH^- ions. For the anodic films considered, of density 3.1×10^3 kg m^{-3}, typical average compositions are:

$$Al_2O_{3.07\pm0.03}B_{0.06\pm0.01}\ (Al_2O_3 0.030 \pm 0.005(B_2O_{2.4\pm1.2}))$$

$$Al_2O_{3.17\pm0.02}P_{0.072\pm0.06}\ (Al_2O_{2.99\pm0.04} 0.074 \pm 0.006(AlPO_4))$$

$$Al_2O_{3.051\pm0.0008}W_{0.0146\pm0.0001}\ (Al_2O_3 0.015 \pm 0.001(WO_{3\pm1}))$$

3.1.2. Film growth at reduced current efficiency

For film growth at high current efficiency, i.e. 100%, the voltage–time response of Fig. 2 reveals a slope of 2.3 V s^{-1} for anodizing at 5 mA cm^{-2}. Interestingly, as the current density employed for anodizing is reduced the slope of the voltage–time curve shows a proportionate reduction; however, below a certain current density, an increased amount of charge is required to achieve a selected voltage, or film thickness, implying a decrease in current efficiency from 100%. With further reduction in current density, the efficiency decreases, until a so-called critical current density is achieved, when a porous anodic film results [24]. Broadly, similar behaviour is evident when the electrolyte pH is reduced from near-neutral levels.

Understanding the previous behaviour is assisted by the observation of the locations of marker layers within the anodic film sections. Thus, Fig. 5 considers anodizing at constant current density in a typical neutral solution (a), and solutions of progressively reduced pH (b) and (c). As the solution pH is reduced, an increasing time and hence, charge are required to form films to the selected final voltage and thickness. Observations of the resultant film sections and associated xenon marker reveals that the implanted xenon location moves outwards, towards the film–electrolyte interface, indicating a progressive reduction in the apparent transport number of aluminium cations. Indeed, at the so-called critical current density, the marker is located in the alumina film material adjacent to the film–electrolyte interface, implying an apparent cation transport number of zero.

Parallel studies of the electrolyte composition for anodizing under the conditions of Fig. 5 revealed the absence of aluminium ions in solution for condition (a), with aluminium

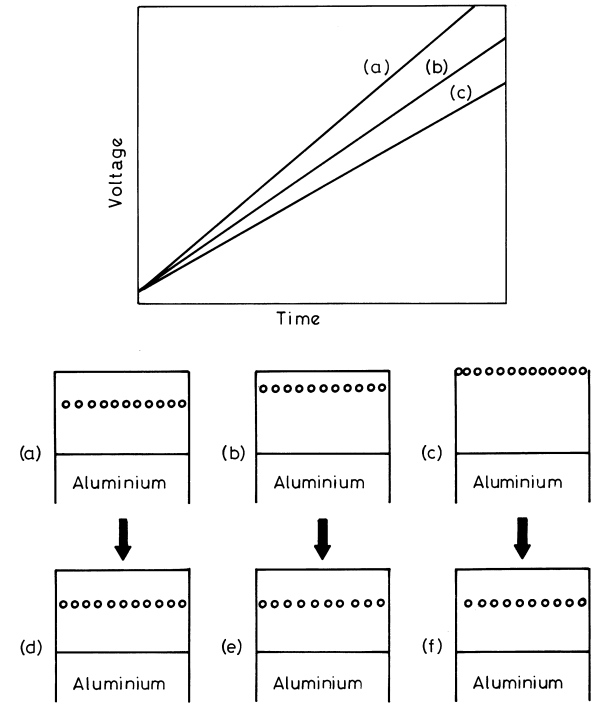

Fig. 5. Schematic diagram showing influence of reduced current efficiency of film formation ((a)–(c)) on the voltage–time response and position of an implanted marker in the film section. At 100% current efficiency, for anodizing at 5 mA cm^{-2}, the slope of the *V–t* curve of (a) is 2.3 V s^{-1}; this reduces to about 1.4 V s^{-1} (c) prior to porous anodic film formation.

ions detected in solution for (b), and with an increased concentration for (c). Further, if the aluminium ion concentration in solution is transformed into an effective film thickness, the marker would be located at the usual position for film growth at high current efficiency, i.e. at a location of 0.4 of the film thickness measured from the film–electrolyte interface (Fig. 5(d)–5(f)).

Direct interpretation thus indicates that, for all growth conditions, Al^{3+} egress and O^{2-}/OH^- ingress occur under the high field. However, the fate of the outwardly mobile Al^{3+} ions at the film–electrolyte interface depends upon the particular interfacial conditions. Thus, at high current efficiency, all outwardly mobile Al^{3+} ions form film material at the film–electrolyte interface; conversely, at the critical current density, all outwardly mobile Al^{3+} ions are ejected directly into the solution from the film–electrolyte interface [24,25]. For intermediate conditions of solution pH and/or current density, a proportion of the outwardly Al^{3+} ions are lost to the electrolyte. Dissolution (chemical) of the alumina film material is relatively insignificant, and the presence aluminium ions in solution results from direct ejection. This is readily tested by reanodizing the film formed under the condition, (c) to increased voltage when the marker remains located at the film–electrolyte interface. If film dissolution per se is important, the marker would have been lost by successive removal of the film material by dissolution proceeding inwards from the film–electrolyte interface.

At the critical current density, when the apparent cation transport number is zero, the alumina film material develops

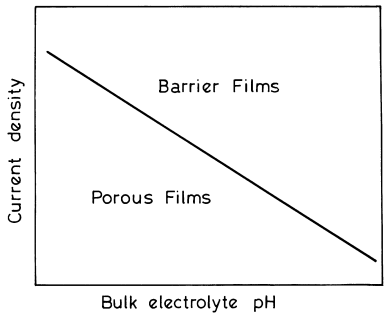

Fig. 6. Schematic diagram showing the relationship between solution pH and current density for barrier or porous-type anodic alumina formation. The current densities are typically in the mA range over a pH range between 0 and 7.

only at the metal–film interface through O^{2-}/OH^{-} ingress; as indicated previously, Al^{3+} cations are outwardly mobile, in their co-operative manner with anions, but no solid alumina is formed at the film–electrolyte interface because of their direct ejection to solution. This is a necessary condition for porous anodic alumina formation, otherwise outwardly mobile Al^{3+} ions, forming solid alumina at the film–electrolyte interface, would ''heal'' any developing or embryo pores. Generally, for most anodizing electrolytes, relationships between current density and bulk electrolyte pH exist, delineating porous and barrier or compact film growth (Fig. 6).

3.1.3. Anodic oxidation of aluminium alloys

Clearly, as structural materials, aluminium alloys have wide applications; hence, the various fates of alloying elements during anodic oxidation require consideration. Such a study is assisted by use of sputtered, non-equilibrium alloys, allowing a wide range of alloying elements to be considered.

Broadly, the solid solution alloy behaviour falls into several categories [26]: (i) alloying elements oxidize immediately at the alloy–film interface; (ii) alloying elements enrich at the alloy–film interface prior to their oxidation; (iii) alloying elements enrich without subsequent oxidation and incorporation into the anodic film. In the first category, lithium and magnesium, for example, are oxidized at the alloy–film interface and are mobile outwards in the anodic film. In the second category, e.g. zinc and copper, initial oxidation of aluminium occurs, with the alloying element enriching from about 1 at.% in the bulk to 40 at.% over 1–5 nm immediately below the anodic film prior to oxidation and incorporation into the anodic film. Such alloying elements may have similar, lesser or greater mobility than Al^{3+} ions, giving rise to anodic films of relatively uniform composition or layered films comprising an outer alumina film and inner film containing the alloying element cation or vice versa. In the third category, e.g. gold, the alloying element enriches at the alloy–film interface, with no eventual oxidation and incorporation into the anodic alumina film.

Fig. 7 shows schematically the section of an alloy and its anodic oxide, where initial oxidation of aluminium leads to

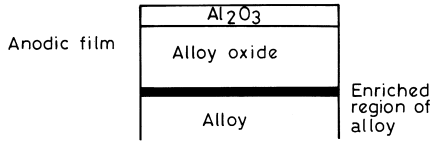

Fig. 7. Schematic diagram of the sectional appearance of a barrier film formed on an aluminium alloy; in this case, the alloying element enriched at the alloy/film interface prior to oxidation and incorporation on the alumina film.

enrichment; subsequent of the alloying element enriched layer produces cations of reduced mobility compared with Al^{3+} cations, i.e. W^{6+} cations.

The previous behaviour correlates relatively well with the heat of formation per equivalent of the relevant oxide, with low values relative to Al_2O_3 indicating no enrichment prior to oxidation at the alloy–film interface; oxides with values above that for Al_2O_3 initially enrich and those with high values only enrich at the alloy–film interface. Relative mobilities of the alloying element cations within the anodic film also correlate to some extent with the single M–O bond energies and the influence of the electric field on bond disruption.

The precise alloy behaviour, described briefly above, also requires consideration of Pilling–Bedworth ratios, mobilities of alloy cations relative to aluminium ions and field strengths within the various film regions as well as the features given previously. For example, in certain cases, void development is evident at the alloy–film interface, oxygen gas evolution proceeds and significant flaw or defect generation is evident within the thickening anodic oxide. Further, discontinuous oxidation of the alloying element from within the enriched layer is evident, possibly suggesting initial cluster development in the alloy substrate.

Concerning the alloying element oxidation from the enriched layer, the use of so-called superimposed metal layers, i.e. tantalum above aluminium or aluminium above tantalum is relevant. In the first case, anodic oxidation develops initially anodic tantala beneath which aluminium is anodized to develop anodic alumina. However, in the case of aluminium above tantalum, anodic alumina formation is followed by preferred penetration of anodic tantala through the alumina film, effectively developing short circuit pathways. Pringle [27] has explained such behaviour on the basis of anodic oxide resistivity, with preferential penetration occurring where an oxide of reduced resistivity penetrates an oxide of increased resistivity. In the reverse situation, conservation of the oxide layers is revealed.

In the case of second-phase material, such material may oxidize, giving oxides of locally altered composition and thickness, with a zone of influence into the surrounding alumina and, depending on the particle geometry and its rate of oxidation, significantly altered anodic film–substrate geometry in local regions.

3.2. Porous-type anodic alumina films

The steady-state porous anodic film of Fig. 1(b) is developed readily by galvanostatic anodizing in acid electrolyte,

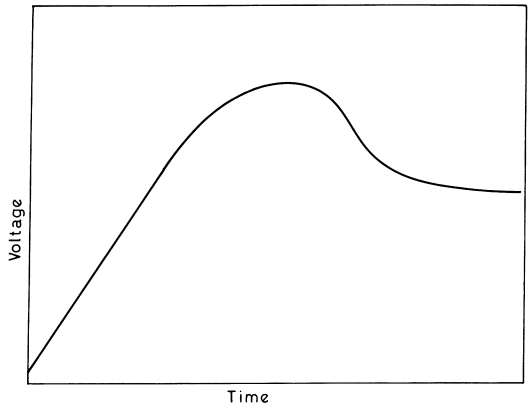

Fig. 8. Typical voltage–time curve for anodizing aluminium at constant current density in an acid electrolyte. For anodizing in 0.4 phosphoric acid, at 25 °C the voltage maximum is about 120 V for a current density of 5 mA cm^{-2}, the maximum is achieved after 180 s.

when the voltage–time curve of Fig. 8 results [6]. Similar films may be formed by anodizing under conditions of constant voltage, and acid or alkaline electrolytes may be employed. The growth, morphology and composition of porous anodic films on aluminium have received widespread attention, with the various stages in their development observed and it is known that the major anodic film parameters (barrier layer thickness and pore and cell diameters) are directly dependent upon the steady-state voltage [6]. Given this information, it is possible to tailor-make films of controlled morphology and composition, or more precisely and within certain limits, incorporation of electrolyte species.

3.2.1. Pore initiation

From consideration of barrier-type anodic films, the concept of a critical current density was introduced, below which no contribution to solid film growth is evident at the film–electrolyte interface. Hence, the film developed at the metal–film electrolyte interface experiences the electrolyte where, at preferred sites, it eventually undergoes dissolution, assisted by the electric field [24]. Interaction with the electrolyte results in the development of penetration paths from the outer film surface, which are the precursors of the regular pores. Since all outwardly mobile Al^{3+} species are lost to the electrolyte without forming solid film material, no mechanism exists to heal the initial penetration paths and the eventual development of the porous anodic film.

For the conditions given, i.e. anodizing of aluminium in chromic acid [24], the potential distribution has been determined during the initial stages of film growth and development of penetration paths, with a finite-element method of numerical analysis adopted to solve the appropriate mathematical expressions for the field distribution. For the initially developed, relatively uniform film (Fig. 9(a)), a uniform potential distribution is revealed across the film section. However, with the development of penetration paths (Fig. 9(b) and 9(c)), the potential lines remain relatively uniformly separated within the compact region of film but, immediately beneath the paths, the potential lines are concentrated, indicating a local increase in field strength. For the more advanced penetration paths, there is a consequent increase in local field strength, enhancing their development through field-assisted dissolution; field-assisted dissolution effectively polarizes the Al–O bonds, allowing more ready Al^{3+} dissolution than in the absence of the field. The eventual development of the penetration paths into the readily recognised pores arises, which is assisted by the relatively strong lateral component of the field beneath the tip of the penetration path, resulting in its lateral expansion to develop an embryo pore with the characteristic inversely funnelled sectional appearance.

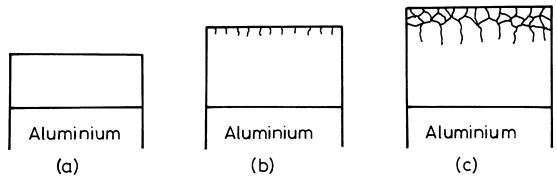

Fig. 9. Schematic diagram illustrating the development of penetration paths, the precursors to pores, during anodizing in chromic acid.

As a consequence of pore development, the electric field and ionic current become concentrated in the barrier layer beneath the major pores. This implies continued ingress of O^{2-}/OH^{-} ions to form solid film at the metal–film interface and corresponding Al^{3+} ejection at the pore base–electrolyte interface as well as field-assisted dissolution of Al^{3+} ions, unlike the relatively low field strength regions between developing pores. Consequently, in the regions of current concentration, a localized scalloping of the metal–film interface occurs. This trend continues until the scalloped regions merge and, thereafter, the steady-state anodic film morphology is created.

The development of penetration paths and, ultimately, pores arises from the concentration of the field beneath and closely adjacent to them. The concentration of field and hence current, results in the so-called field-assisted dissolution of the film material which is probably thermally enhanced through local Joule heating effects. From the mathematical analysis mentioned previously, electrostriction pressures may be calculated at various locations in the film section. Immediately below fine penetration paths, values of about 19×10^7 kg m^{-2} are calculated, whereas between penetration paths the values are around 21×10^4 kg m^{-2}. Compared with the critical compressive stress of the anodic film ($\sim 10^7$ kg m^{-2}), the significantly increases values beneath penetration paths gives credence to Al–O bond polarization and weakening, as suggested for field-assisted dissolution. Field-assisted dissolution may proceed typically at a rate of 300 nm min^{-1} compared with chemical dissolution rates of alumina in the absence of the field at about 0.1 nm min^{-1} at room temperature.

In the previous case, porous anodic oxide formation in chromic acid was employed; however, detailed observation of porous film formation in phosphoric acid has been considered more extensively [28]. From assessment of the voltage–time behaviour during anodizing in phosphoric acid, it is

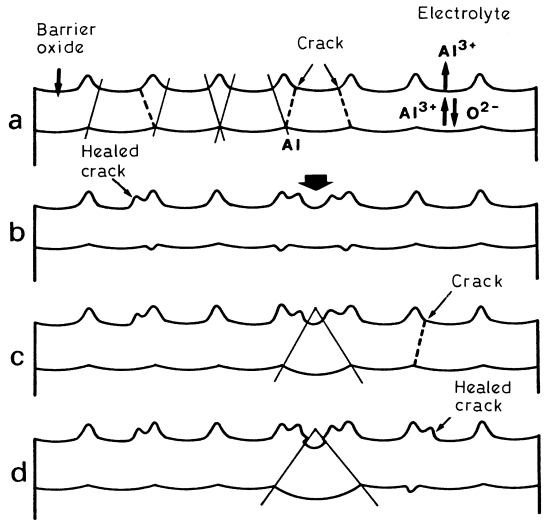

Fig. 10. Schematic diagram showing pore development during anodizing of aluminium in phosphoric acid.

evident that the current efficiency in the early stages of anodizing in phosphoric acid is about 54% that of film formation under similar conditions, but in neutral electrolyte. Thus, film growth in phosphoric acid is associated with considerable loss of Al^{3+} ions from the onset of anodizing, as expected. Observation of films formed on electropolished aluminium reveal non-uniform thickening of the oxide as the voltage rises, with thicker oxide developing above the ridges of the cellular texture which results from electropolishing, with protuberances extending from the outer surface of the anodic film (Fig. 10). A direct outcome is that the planarity of the typical barrier film is lost, with the local film surfaces between the protuberances exhibiting distorted, hemispherical curvatures. In the thin areas between protuberances, where the current for film formation largely flows, the film material is largely of uniform thickness in the direction perpendicular to the local film surface. Importantly, the metal–film interface reveals occasional local regions closely-associated with the metal ridges, where crack–heal events appear to have taken place. Above such regions, protuberances of locally thicker film material appears distorted by the rapid healing of cracks at high local current density. With further film growth, the protuberances become more pronounced, whilst the overall film thickness increases and the curvature of the film surfaces between protuberances increases.

For film growth in phosphoric acid, non-uniform film thickening is evident, unlike typical barrier film formation in neutral solution; furthermore, the local thickening of the oxide becomes more pronounced as the forming voltage rises. For anodizing in phosphoric acid, at an initial efficiency of 54%, it is evident that the Pilling–Bedworth ratio effectively falls from 1.71 (for highly current efficient barrier-film formation) to about 0.91. An inevitable, but important, consequence of this is that the planarity of the alumina film surface becomes unstable with respect to perturbations and the film thickness under tensile stress. Further, the oxide growth kinetics require the film to be of uniform thickness in a direction perpendicular to the local film surface, or the oxide–electrolyte interface, where the current for film formation flows. Thus, the local geometrics of the metal–oxide interface are now determined by those of the corresponding oxide–electrolyte interfaces.

Using the previous findings, films on electropolished aluminium thicken non-uniformly because of local crack–heal events at the pre-existing metal ridges; this causes redistribution of current and its concentration into the thin film regions between protuberances. The local film surfaces in these areas exhibit appreciable hemispherical curvatures of varying radii; also, with further increase in voltage, the protuberances become wider, due to persistent crack–heal events, increasing the curvature of the film–electrolyte interface in the thin film regions. The increasing curvature increases the field in the previous thinner film regions to a level where the field-assisted dissolution rate is equal to the rate of thickening of the oxide at the metal–film interface due to inward migration of O^{2-} ions. A further outcome of the previous reasoning is that regions of locally thinner film material of increased curvature between the protuberances develop major pores earlier than regions of reduced curvature. Further, if substrates of different pretreatments are employed, i.e. electropolishing and scratching, regions of initial preferred pore development are established as a result of the geometry or curvature of the local film surface.

3.2.2. Steady-state porous anodic film

For the steady-state film displayed in the schematic diagram of Fig. 11, the average field across the barrier layer dictates the film growth, with the locally increased field at the pore base–electrolyte interface influencing field assisted dissolution. Calculations by Xu [24] suggest an average field strength of 8×10^{6} V cm^{-1} and a local, increased field strength of 2×10^{7} V cm^{-1}. Clearly, for steady-state film growth, there is a dynamic equilibrium between film growth at the metal–film interface and field-assisted dissolution at the pore base–electrolyte interface. Further, electrolyte species are adsorbed at the pore base–electrolyte interface, and inwardly mobile species are incorporated into the porous anodic film material (Fig. 11). Conversely, immobile or outwardly mobile species, discussed earlier for barrier-type

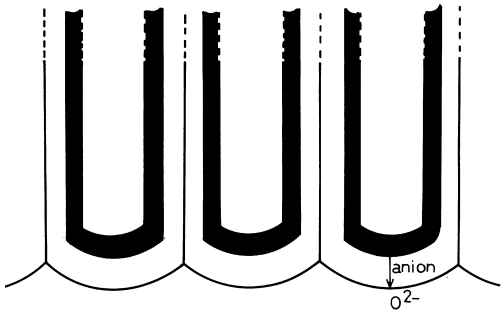

Fig. 11. Schematic diagram of the porous anodic film section, showing region of anion incorporation (shaded). For anodizing in phosphoric acid, the region of anion incorporation extends about two-thirds of the barrier layer thickness.

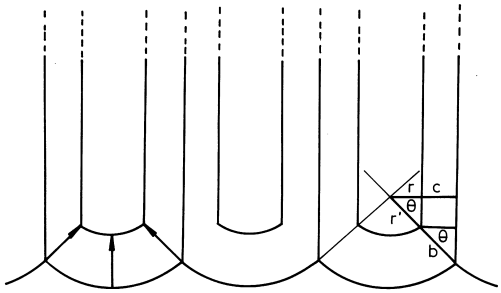

Fig. 12. Geometric model of the steady-state porous anodic film.

anodic film formation, have no means of incorporation. Thus, relatively stable anion species are incorporated into porous anodic films, with typical levels being 12–14 wt.% sulphate, 6–8 wt.% phosphate and 2.4 wt.% oxalate [29].

For a porous anodic film formed into the steady-state region in phosphoric acid, the section close to the metal is shown schematically in Fig. 12. From measurements of the film parameters, relationships between them are established, i.e.

$$\theta = \cos^{-1}\left(\frac{\text{pore radius } (r)}{\text{pore base radius of curvatures } (r^1)}\right)$$

$$= \cos^{-1}\left(\frac{\text{cell wall thickness } (c)}{\text{barrier layer thickness } (b)}\right)$$

Further, since of the major parameters are proportional to the steady-state voltage, films formed under different voltages have the same porosity. This follows because the cross-section area of the pore is proportional to V^2 whilst the pore population density is proportional to V^{-2}.

Under steady-state conditions, when the voltage does not change with time, the resultant anodic film parameters remain unchanged. This results from a self-adjusting situation, where any tendency for the pore diameter to increase or decrease is checked by a consequent increase or decrease in the radius of curvature of the pore base. Thus, in essence, film formation occurs at a constant rate, being determined by the average field. It is balanced by field-assisted dissolution, at a rate determined by the local field, related to the radius of curvature of the pore base.

Observations of porous anodic film surfaces and cell-base patterns in the metal after oxide stripping reveal a greater pore population density at the surface. This arises from incipient pores which develop initially but are surplus to the requirement of the field and cease to function. For normal growth conditions, the steady-state pores are cylindrical in section and remain unchanged in diameter with anodizing time. Close to the film surface, such pores are inversely funnelled, reflecting their initial development. Under certain situations, normally-funnelled pores may develop, particularly when the influence of chemical dissolution on the alumina film material is enhanced, i.e. by anodizing at sufficiently high temperature.

4. Concluding remarks

From the previous considerations it is evident that an armoury of techniques is available for characterization of anodic alumina films on aluminium; for example, morphological examination is assisted greatly by direct observation of the amorphous film material at appropriate magnification by transmission electron microscopy. Film composition may be probed with sufficient sensitivity by RBS, AES, XPS and XAS, assisted by the use of appropriately generated markers and tracers. The amorphous alumina structure itself is amenable to probing by XAS, with XANES and EXAFS data indicating largely that as-formed films reveal only four- and five-fold co-ordination of aluminium with oxygen; the appearance of single shells in the Fourier transformed data suggest strongly the amorphous nature of the films. Given information of the previous kind, it is essential to now probe the detailed ionic transport mechanism under the high-field, where Al^{3+} and O^{2-}/OH^- ions migrate across the thickening alumina film material.

Applications of the alumina films include largely dielectrics in electronic uses for barrier films, with appropriate surface area magnification by tunnelling of the aluminium substrate. Porous anodic films on aluminium are available for decorative, wear-resistant and corrosion-resistant applications. Thus, the porous skeleton may be penetrated, at least partly, by organic dyestuffs or inorganic pigments (by double decomposition reactions) to provide coloured, decorative finishes. Alternatively, metal or alloy pigments may be built up from the individual pore bases to provide durable decorative products. After such treatments, the anodic films are sealed by hydrothermal treatment in boiling water, which blocks the pores and bridges over the inevitable defects or flaws in the film, hindering environmental access to the substrate and, consequently, imparting corrosion resistance to the substrate.

For tribological enhancement of aluminium, wear resistance is improved by anodizing, particularly if so-called hard anodizing is employed, using low temperature electrolytes.

Other applications include magnetic storage devices, whereby porous films are formed on highly flat substrates; the pores are then widened in a controlled manner and magnetic alloys are deposited within the porous skeleton. Porous anodic films may also be used to provide synthetic ruby and polarize light under appropriate conditions.

A major use of porous anodic films is in keying layers for organic adhesives, primer coats and paint finishes. In addition to providing initial adhesion and bond durability, the finished system also retards corrosion in crucial situations, e.g. aerospace applications.

Finally, whilst the previous list is not exhaustive, three other applications are mentioned; suitably released from the aluminium substrate, the free-standing alumina film may be used as a membrane. Further, during anodizing of selected alloys, or by using particular electrolytes, electroluminescence is observed during anodizing; clearly, at present, this is of limited value, since it only proceeds during film growth.

Lastly, the porous alumina material, sufficiently modified, or tailor-made, may be penetrated by many various materials, perhaps providing novel devices for future consideration.

References

[1] S. Wernick, R. Pinner and P.G. Sheasby, *The Surface Treatment and Finishing of Aluminium and its Alloys*, Finishing Association, Teddington, 1987.
[2] L. Young, *Anodic Oxide Films*, Academic Press, New York, 1971.
[3] J.P.S. Pringle, *J. Electrochem. Soc., 119* (1972) 482.
[4] F. Brown and W.D. Mackintosh, *J. Electrochem. Soc., 120* (1973) 1096.
[5] K. Kobayashi, K. Shimizu, G.E. Thompson and G.C. Wood, *J. Appl. Electrochem., 15* (1985) 781.
[6] J.P. O'Sullivan and G.C. Wood, *Proc. Roy. Soc. London, A317* (1970) 511.
[7] G.C. Wood, P. Skeldon, G.E. Thompson and K. Shimizu, *J. Electrochem. Soc., 143* (1996) 74.
[8] M. Paez, T.M. Foong, C.T. Ni, J. Habazaki, K. Shimizu, P. Skeldon, G.E. Thompson and G.C. Wood, *Corros. Sci., 38* (1996) 59.
[9] G.E. Thompson, P. Skeldon, G.C. Wood, K. Shimizu and S.H. Han, *Philos. Mag., 55* (1987) 651.
[10] K. Shimizu, G.E. Thompson, G.C. Wood and Y. Xu, *Thin Solid Films, 88* (1982) 255.
[11] R.C. Furneaux, G.E. Thompson and G.C. Wood, *Corros. Sci., 18* (1978) 853.
[12] P. Skeldon, K. Shimizu, G.E. Thompson and G.C. Wood, *Surf. Int. Anal., 5* (1983) 247, 252.
[13] Y. Xu, G.E. Thompson and G.C. Wood, *Corros. Sci., 27* (1987) 83.
[14] J. Robinson, G.E. Thompson, K. Shimizu, K. Hebert and G.E. Thompson (eds.), *Oxide Films on Metals and Alloys*, Proc. Vol. 94–25, The Electrochemical Society Inc., Pennington, NJ, 1994.
[15] I. Farnan, R. Dupree, Y. Jeong, G.E. Thompson, G.C. Wood and A.J. Forty, *Thin Solid Films, 173* (1989) 209.
[16] N. Cabrera and N.F. Mott, *Rep. Prog. Phys., 12* (1948–1949) 163.
[17] K. Shimizu, K. Kobayashi, G.E. Thompson and G.C. Wood, *Philos. Mag. B, 64* (1991) 345.
[18] P. Skeldon, K. Shimizu, G.E. Thompson and G.C. Wood, *Philos. Trans. Roy. Soc., A348* (1994) 295.
[19] C. Cherki and J. Siejka, *J. Electrochem. Soc., 120* (1973) 784.
[20] G. Amsel and D. Samuel, *J. Phys. Chem. Solids, 23* (1962) 1707.
[21] N.F. Mott, *Philos. Mag. B, 55* (1987) 117.
[22] M. Skeldon, P. Skeldon, K. Shimizu, G.E. Thompson and G.C. Wood, *Philos. Mag., 60* (1989) 513.
[23] P. Skeldon, K. Shimizu, G.E. Thompson and G.C. Wood, *Thin Solid Films, 123* (1985) 127.
[24] Y. Xu, *Ph.D. Thesis*, University of Manchester, 1983.
[25] J. Siejka and C. Ortega, *J. Electrochem. Soc., 124* (1977) 883.
[26] P. Skeldon, H. Habazaki, K. Shimizu, X. Zhou, G.E. Thompson and G.C. Wood, *Nature*, submited.
[27] J.P.S. Pringle, *Electrochim. Acta, 25* (1980) 1403.
[28] K. Shimizu, K. Kobayashi, G.E. Thompson and G.C. Wood, *Philos. Mag. A, 66* (1992) 643.
[29] C. Alvey, *Ph.D. Thesis*, University of Manchester (1978).